Room-Temperature Weak Ferromagnetism Induced by Point Defects in α-Fe_2O_3

Jiangtao Wu,[†] Shaoyu Mao,*[,†] Zuo-Guang Ye,[‡] Zhaoxiong Xie,*[,†] and Lansun Zheng[†]

State Key Laboratory for Physical Chemistry of Solid Surface & Department of Chemistry, College of Chemistry and Chemical Engineering, Xiamen University, Xiamen 361005, China, and Department of Chemistry and 4D LABORATORIES, Simon Fraser University, 8888 University Drive, Burnaby, British Colombia, V5A1S6 Canada

ABSTRACT Unusual room-temperature weak ferromagnetism α-Fe_2O_3 was prepared by heating the mixture of commercial α-Fe_2O_3 (as raw material) and tartaric acid at a mild temperature of 250 °C. This reaction involves a fast heating and cooling process resulting from the self-catalyzed oxidation of tartaric acid. Careful chemical analyses confirmed that no any ferromagnetic impurities, such as Fe, Fe_3O_4, amorphous iron oxide and γ-Fe_2O_3, were present in the treated sample. The unusual weak ferromagnetism was then attributed to the formation of a large amount of point defects in the treated sample during the peculiar synthetic process. Such a mechanism is supported by the result of annealing, which reduces the amount of point defects and thereby reestablishes the original antiferromagnetism in α-Fe_2O_3.

KEYWORDS: hematite • catalyzed oxidation • ferromagnetism • point defect

INTRODUCTION

Recently, unusual ferromagnetism was found in some traditionally nonmagnetic materials. For examples, ferromagnetic property was unexpectedly found in the HfO_2 thin film, in which intrinsic point defects were thought to be responsible for the ferromagnetism (1, 2), room-temperature ferromagnetism was observed in ZnO films due to the defects of Zn vacanies (3), Al-doped ZnO-Al nanostructure also exhibited ferromagnetism due to charge transfer (4), and surface reconstruction could induce surface magnetization in nondoped ZnO nanostructures (5). From the view points of both fundamental research and applications, exploration of new kinds of materials with unusual ferromagnetism and understanding of its mechanism are of great importance.

Hematite Fe_2O_3 is an antiferromagnet with a Néel temperature of 950 K. It possesses a corundum-type structure with the space group of $R\bar{3}c$. The arrangement of magnetic moments in α-Fe_2O_3 in the temperature range of 250−950 K leads to the so-called spin-canted magnetism, in which the Fe^{3+} spins are aligned perpendicular to the *c*-axis (6, 7). In this letter, we report the finding of unusual weak ferromagnetism in the originally antiferromagnetic hematite Fe_2O_3 (α-Fe_2O_3) at room temperature. The ferromagnetic α-Fe_2O_3 was prepared from commercial hematite powder by a self-catalyzed oxidation reaction in the presence of tartaric acid. The mechanism of the weak ferromagnetism is attributed to the large amount of point defects formed during the local fast heating and rapidly cooling process during the reaction.

* Corresponding author. E-mail: symao@xum.edu.cn (S.M.); zxxie@xmu.edu.cn (Z.X.).

Received for review March 10, 2010 and accepted May 17, 2010

[†] Xiamen University.

[‡] Simon Fraser University.

DOI: 10.1021/am1002052

EXPERIMENTAL SECTION

Weak ferromagnetic α-Fe_2O_3 was obtained by heating the mixture of α-Fe_2O_3 (99%, Alfa Aesar) and tartaric acid ($C_4H_6O_6$, 99.5%, Alfa Aesar). In a typical synthesis, 0.5 mmol of iron oxide and 5 mmol of tartaric acid were mixed in an agate mortar, and a few drops of ethanol were used to serve as abrasive. The mixture was then put in a ceramic crucible and heated to about 250 °C in air by a heating jacket, at which it began to ignite and violently burn. The combusting process lasted for a few seconds. After complete combustion, the product was naturally cooled to room temperature. The treated sample was obtained and its magnetic properties were characterized by means of a superconducting quantum interference device (SQUID, Quantum Design, USA). The XRD measurements were carried out on a PANalytical X-ray diffractometer using Cu Kα radiation, and a Hitachi S4800 field-emission scanning electron microscope was used to determine the morphology of the samples. X-ray photoelectron spectroscopy (XPS, PHI660) using a monochromatic Mg Kα X-ray source, where the binding energies were calibrated with respect to the signal for adventitious carbon (binding energy of 284.6 eV). Differential thermal analyses (DTA/TGA) were carried out on a simultaneous TGA/DSC apparatus (SDT Q600, TA Instruments-Waters LLC, USA) at a heating rate of 5 °C/min in air.

RESULTS AND DISCUSSION

Figure 1a shows the variation of the magnetization *M* as a function of magnetic field *H* of the treated sample at 300 and 2 K, and that of the commercial α-Fe_2O_3 (i.e., the raw material) for comparison. It can be seen that, as expected, the commercial α-Fe_2O_3 exhibits a typical antiferromagnetic behavior. In contrast, the treated sample displays a slim but well-defined magnetic hysteresis loop with a remanent magnetization of 1.9 emu/g at 300 K, 5.5 emu/g at 2 K, respectively. The magnetization is saturated at a small field

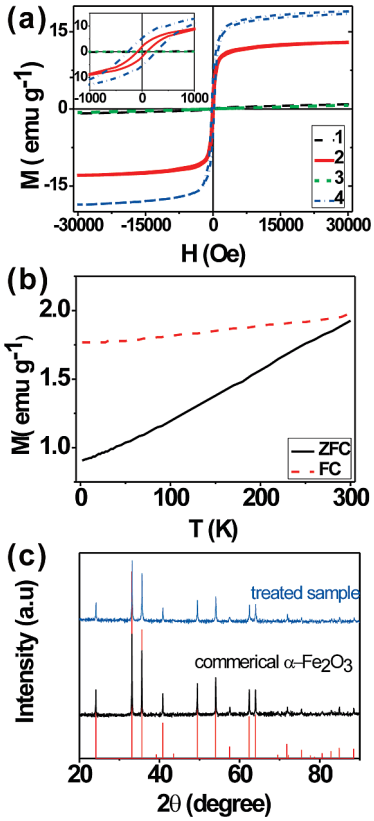

FIGURE 1. (a) Magnetization (M) versus field (H) curves for the commercial (raw) α-Fe_2O_3 powder and the treated sample at 300 and 2 K. The inset shows the detail of the $M-H$ curve displayed at $\pm$1000 Oe: (1) commercial α-Fe_2O_3 at 300 K; (2) treated sample at 300 K; (3) commercial sample at 2 K; (4) treated sample at 2 K. (b) Zero-field-cooled (ZFC) and field-cooled (FC) magnetization measured at a field of 100 Oe below room temperature. (c) XRD patterns of the commercial α-Fe_2O_3 (lower) and the treated sample (upper). The red line represents the standard powder diffraction data of α-Fe_2O_3 (JCPDS Card No. 33−0664).

strength of about 1000 Oe, with a saturation magnetization of 12.2 emu/g at 300 K and 18.9 emu/g at 2 K. The treated sample has a small coercive filed of 95 Oe at 300 K and 276 Oe at 2 K. This magnetic hysteresis loop indicates that the treated α-Fe_2O_3 powder is weak ferromagnetic at room temperature. Figure 1b gives the temperature dependences of the ZFC and FC magnetizations at 100 Oe, which exhibit different values below 300 K. The difference becomes more significant at lower temperatures, with the FC magnetization being higher than the ZFC one.

To investigate the intrinsic difference between the treated sample and the commercial α-Fe_2O_3, structural and morphologic characterizations were carried out by using the X-ray diffraction (XRD) technique and the scanning electron microscopy (SEM). As shown in Figure 1c, the treated sample exhibits the same XRD pattern as the commercial α-Fe_2O_3, indicating that it indeed belongs to the hematite phase of α-Fe_2O_3 (JCPDS Card No. 33−0664) with the $R\bar{3}c$ space group, without any impurity phase. The crystal size of the treated sample is larger than 100 nm, as estimated by the Scherrer formula. However, the SEM images show the morphologies of the two corresponding samples are completely different: the raw α-Fe_2O_3 sample contained particles of regular spherical shape (Figure 2a), which have turned into

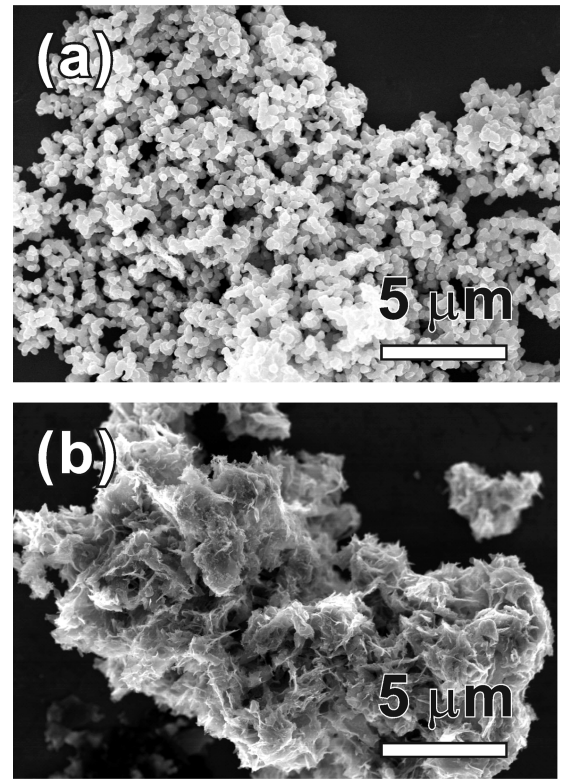

FIGURE 2. (a, b) SEM images of the commercial and treated sample, respectively.

flowerlike clusters (Figure 2b) after the reaction. This indicates that the α-Fe_2O_3 was melted during the reaction, which implies that local temperature has reached very high as a result of the catalyzed oxidation of tartaric acid in the presence of α-Fe_2O_3. The catalyzed oxidation process can be described by the following chemical equation

$$C_4H_6O_6(s) + 5/2O_2(g) \xrightarrow{\alpha\text{-}Fe_2O_3,\ 250\ ^\circ C} 4CO_2(g) + 3H_2O(g) + \text{Heat} \quad (1)$$

This fast combustion process is different from the conventional self-propagating combustion method (8), mainly in that it involves a self-catalyzed oxidation. It is well-known that some carbohydrates such as tartaric acid, glycin, sucrose, etc., could not burn in air at low temperature. Instead, they first carbonize into carbon, and then begin to burn at much higher temperature. However, with the help of a solid-state catalyst, for instance, iron oxide, these organic compounds can react strongly, at a relatively low temperature, with activated oxygen molecules that are absorbed on the surface of metal oxide catalyst, giving out a great deal of heat (9). It is plausible that such a catalyzed reaction could raise the local temperature in the sample to above the melting point (1560 °C) of α-Fe_2O_3 in a few seconds, which then dropped down rapidly after the reaction was over. Such a fast heating and cooling process could induce a considerable amount of point defects in the treated α-Fe_2O_3.

To investigate the origin of the ferromagnetism, the composition of both the commercial and treated α-Fe_2O_3

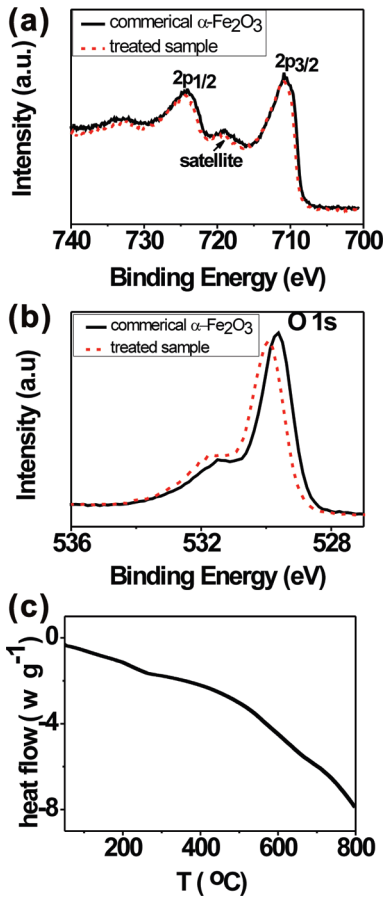

FIGURE 3. (a) XPS spectra of Fe 2p core levels of the commercial and treated α-Fe_2O_3 samples. (b) XPS spectra of O 1s level of the commercial and treated α-Fe_2O_3 samples. (c) DTA curve of the treated sample.

samples were carefully determined by XPS. The XPS spectra of the Fe 2p core levels permit determination of any changes in the surface composition of the treated α-Fe_2O in terms of binding energy, compared with the commercial α-Fe_2O_3. Figure 3a presents the XPS spectra of the two samples. The two samples exhibit almost the same spectra with Fe 2p core levels binding energy of 711.0 eV (Fe $2p_{3/2}$) and 724.1 eV (Fe $2p_{1/2}$), corresponding to those of Fe^{3+}. The Fe $2p_{3/2}$ peak is also associated with a satellite peak located at 719.0 eV, which is the characteristic peak for the α-Fe_2O_3 phase (10). Other reduced states, such as Fe^{2+} and Fe^0, cannot be found in the XPS spectrum (11), indicating the absence of any other possible ferromagnetisms like Fe, FeO or Fe_3O_4. In addition, differential thermal analysis (DTA) was carried out to determine the presence of any amorphous iron oxide in the treated α-Fe_2O_3. As shown in Figure 3c no exothermic peak in the temperature range of 50−800 °C can be observed,. According to the literature, two well-resolved exothermic peaks should be observed in the DTA curves of amorphous Fe_2O_3 (12). The first peak at 292 °C is attributed to the crystallization of amorphous Fe_2O_3 to γ-Fe_2O_3, whereas another one, being more intensive and occurring at 396 °C, corresponds to the polymorphous isochemical transformation of γ-Fe_2O_3 to α-Fe_2O_3. The absence of these two peaks indicates that no amorphous iron oxide or γ-Fe_2O_3 was presented in the treated α-Fe_2O_3. Figure 3b presents the XPS spectra of O 1s level of the two samples. The binding energy of the treated sample (530.0 eV) is slightly higher than commercial sample (529.6 eV). This indirectly proves the formation of oxygen defects in the treated α-Fe_2O_3, as with oxygen deficiency, it needs a relatively higher energy to stimulate oxygen atoms, resulting in a higher binding energy compared to the commercial sample (raw material).

The above experimental results suggest that the unusual weak ferromagnetism in the treated α-Fe_2O_3 cannot be associated with any impurity phases, such as Fe, FeO, Fe_3O_4, γ-Fe_2O_3, and amorphous Fe_2O_3, which have been excluded from the sample. Instead, it can be attributed to the defects formed in the α-Fe_2O_3, which were induced during the fast heating and cooling process. Recently, it was revealed by several researchers that point defects of oxygen vacancies could result in ferromagnetism (5, 13), and the magnetization in the ferromagnetic $M(H)$ curve could be enhanced by increasing oxygen vacancies (14). The magnetic property of α-Fe_2O_3 was also investigated both by calculation and experiment (15−17). In the process of the catalyzed oxidation reaction developed in this work, the α-Fe_2O_3 prepared following the extremely fast heating and cooling process is expected to contain a considerable amount of point defects. According to the previous works about the point defects both on the surface and in the bulk of hematite (18−20), the value of the enthalpy of formation of iron interstitials is similar to that of oxygen vacancies, suggesting that both species play important roles in the defect structure. The calculations by Warschkow et al. (15) revealed the stabilization of oxygen vacancies in the two oxygen layers closest to the surface, suggesting an increased concentration of oxygen vacancies near the surface. It is reasonable to postulate that these point defects could destroy the antiferromagnetic superexchange interaction of $Fe^{3+}-O^{2-}-Fe^{3+}$. resulting in uncompensated magnetization and thereby the ferromagnetic order. This proposed mechanism of point defect-induced ferromagnetism in α-Fe_2O_3 is supported by the result of thermal annealing experiment. When the treated sample was heated in air at 650 °C for 2 h and cooled to room temperature upon natural oven-cooling, the weak ferromagnetism of the sample disappeared and instead it exhibited typical antiferromagnetism (Figure 4b). Figure 4a gives the XRD pattern of the annealed sample, indicating that it remained to be α-Fe_2O_3. However, its magnetization became very small (<1 emu/g) and could not be saturated even at a field of as strong as 30 000 Oe, which is the same behavior as the commercial α-Fe_2O_3 (curve 1 in Figure 1a). The annealing process reduces the amount of point defects significantly, and thus reestablishes the original antiferromagnetism in α-Fe_2O_3. Therefore, the treated weak ferromagnetic α-Fe_2O_3 powder must exist in a new metastable state with a considerable amount of point defects. Figure 4c shows the SEM image of the annealed sample, which shows that its crystal size (>100 nm) and morphology were not changed during the annealed process. As first noted by Néel, antiferromagnetic nanoparticles could exhibit superparamagnetic relaxation of their spin−lattices as well as permanent moment arising from

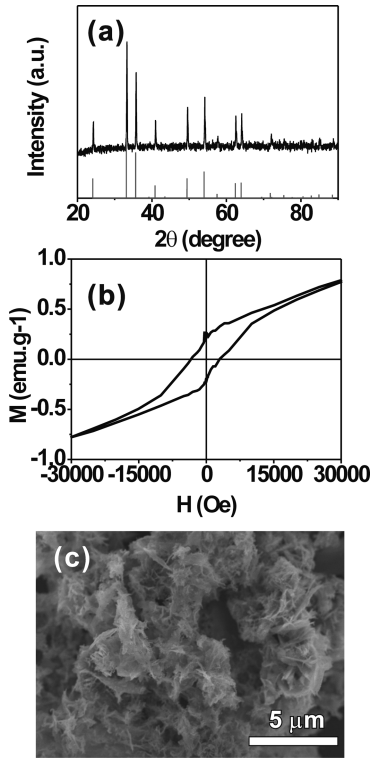

FIGURE 4. (a) XRD patterns of the (initially) treated α-Fe_2O_3 sample after being annealed at 650 °C in air for 2 h. The Red line represents the powder data of JCPDS Card No. 33−0664. (b) Magnetization (M) versus field (H) curve for the annealed α-Fe_2O_3 sample at 300 K. (c) SEM images of the annealed α-Fe_2O_3 sample.

uncompensated surface spins. However, in this work, we found that both the crystal size and surface remain the same before and after annealing process, while the magnetic behavior changes dramatically. The crystal sizes of the treated sample and annealed sample are both larger than 100 nm, as estimated by the Scherrer formula from XRD pattern, and confirmed by the SEM imaging. Therefore, the size effect and surface spin are not the primary reason of the unusual magnetic behavior observed.

CONCLUSIONS

In summary, we have developed a self-catalyzed fast solid state reaction technique to prepare α-Fe_2O_3 which exhibits weak ferromagnetic behavior. It is possible to control the concentration of defects by varying different amounts, and kinds, of carbohydrates. Chemical analyses have confirmed that the treated weak ferromagnetic sample belongs to the pure phase of α-Fe_2O_3, without any impurity phases. The ferromagnetism is proposed to arise from the large amount of point defects formed because of the rapid heating and cooling process involved in the reaction. Such a mechanism suggests that other new types of ferromagnets can be prepared by appropriately introducing point defects in the materials. It is naturally expected that the technique developed in this work can be applied to the synthesis of other types of materials to create point defects and thereby to provide unusual properties.

Acknowledgment. This work was supported by the Natural Science and Engineering Research Council of Canada (NSERC), the National Natural Science Foundation of China (Grants 20725310 and 20673085), and the National Basic Research Program of China (Grant 2007CB815303).

REFERENCES AND NOTES

(1) Venkatesan, M.; Fitzgerald, C. B.; Coey, J. M. D. *Nature* **2004**, *430*, 630.
(2) Pemmaraju, C. D.; Sanvito, S. *Phys. Rev. Lett.* **2005**, *94*, 217205.
(3) Xu, Q.; Schmidt, H.; Zhou, S.; Potzger, K.; Helm, M.; Hochmuth, H.; Lorenz, M.; Setzer, A.; Esquinazi, P.; Meinecke, C.; Grundmann, M. *Appl. Phys. Lett.* **2008**, *92*, 082508.
(4) Chen, S. J.; Suzuki, K.; Garitaonandia, J. S. *Appl. Phys. Lett.* **2009**, *95*, 082508.
(5) Schoenhalz, A. L.; Arantes, J. T.; Fazzio, A.; Dalpian, G. M. *Appl. Phys. Lett.* **2009**, *94*, 162503.
(6) Morin, F. J. *Phys. Rev.* **1950**, *78*, 819.
(7) Tasaki, A.; Iida, S. *J. Phys. Soc. Jpn.* **1962**, *16*, 1697.
(8) John, B. W.; Richard, B. K. *Science* **1992**, *255*, 1093.
(9) Jarvis, E. A.; Chaka, A. M. *Surf. Sci.* **2007**, *601*, 1909.
(10) Tahir, A. A.; Wijayantha, K. G. U.; Yarahamdi, S. S.; Mazhar, M.; Mckee, V. *Chem. Mater.* **2009**, *21*, 3763.
(11) Brundle, C. R.; Chuang, T. J.; Wandele, K. *Surf. Sci.* **1977**, *68*, 459.
(12) Zboril, R.; Machala, L.; Mashlan, M.; Sharma, V. *Cryst. Growth. Des.* **2004**, *4*, 1317.
(13) Drashan, C.; Ogale, S. B.; Lofland, S. E.; Dhar, S. *Nat. Mater.* **2004**, *3*, 709.
(14) Zhao, B. C.; Ho, H. W.; Xia, B.; Tan, L. H.; Huan, A. C.; Wang, L. *Appl. Phys. Lett.* **2008**, *93*, 222506.
(15) Mazurenko, V. V.; Anisimov, V. I. *Phys. Rev. B* **2005**, *71*, 184434.
(16) Sandrktskit, L. M.; Kübler, J. *Europhys. Lett.* **1996**, *33*, 447.
(17) Li, Y. Y. *Phys. Rev.* **1956**, *101*, 1450.
(18) Dieckmann, R. *Philos. Mag., A* **1993**, *68*, 725.
(19) Richard, C.; Catlow, A.; Corish, J.; Hennessy, J.; Mackrodt, W. C. *J. Am. Ceram. Soc.* **1988**, *71*, 42.
(20) Warschkow, O.; Ellis, D. E. *J. Am. Ceram. Soc.* **2002**, *85*, 213.

AM1002052